Atomic data for astrophysics. Calculations, benchmarking and distribution

G. Del Zanna

Department of Applied Mathematics and Theoretical Physics University of Cambridge Wilberforce Road, Cambridge, CB3 0WA UK

Abstract. Some recent R-matrix and distorted-wave calculations, done as part of the UK APAP-Network, are presented. They are focused on some ions important for the EUV and the X-rays, in particular for the solar corona. A long-term and novel project to benchmark atomic data against laboratory and astrophysical data is summarised, highlighting new plasma diagnostics. The various ways in which the atomic data are made available to the various communities through e.g. the CHIANTI and the VAMDC EU framework are also presented.

Keywords: atomic data - spectral lines
PACS: see `http://www.aip.org/pacs/index.html`

INTRODUCTION

In astrophysics, high-resolution spectroscopy has evolved significantly in the past several years. More detailed observations are pushing the needs for even more accurate atomic data. The gratings on-board XMM-Newton and Chandra have pushed the needs for atomic data in the X-rays (1–50 Å) and soft X-rays (50–170 Å). In solar physics, most missions have focused on extreme-ultraviolet (EUV) wavelengths, for example with the Hinode EUV Imaging Spectrometer [EIS, see 1, SW: 166–212 Å; LW: 245–291 Å], and the Solar Dynamics Observatory (SDO) Extreme ultraviolet Variability Experiment (EVE), which measures the solar spectral irradiance at 1 Å resolution in the 50–380 Å and 350–1050 Å spectral ranges [2]. Accurate and complete atomic data are needed also to interpret broad-band solar imaging in the EUV (e.g. the SDO Atmospheric Imaging Assembly, AIA, with bands centred around 94, 131, 171, 193, 211, and 335 Å).

A substantial effort was consequently devoted in the past few years to calculate and benchmark new atomic data for coronal ions and EUV wavelengths. One of the aims of the APAP (Atomic Processes in Astrophysical Plasmas: *http://www.apap-network.org*) collaboration, a follow-up of UK Rmax, was the calculation of electron excitation and radiative rates for a number of ions important for astrophysics.

The atomic structure calculations are done using the the program AUTOSTRUCTURE [3]. For the electron scattering calculation, we use the *R*-matrix method [4, 5] in conjunction with the intermediate frame coupling transformation [ICFT, see 6, 7].

Some of the calculations have been done for entire isoelectronic sequences. The work on the F-like ions was published in [8], while that for the Na-like ions was described in [9]. For the Ne-like [10], a large-scale calculation with 209 levels close-coupling expansion was done. The calculation for the Li-like [11] iso-electronic sequence included core- and valence-excitations. The new calculations often include more configuration

interaction than previous ones, and for many ions are the first such calculations.

Specific work on some ions has also been done. For example, the Si X model ion was improved with new excitation data, calculated with a large-scale model. Some new lines have been identified with these resultant excitation data [12]. The Fe XIV model ion was also improved over previous calculations by [13], and showed inconsistencies between the theoretical and experimental cross-section near threshold. New atomic data for Fe VII [14], Fe VIII [15], Fe IX [16], Fe X, [17], Fe XI [18], Fe XII [19], Fe XIII [20] have been produced. All the above ions are emitting most of the lines in the Hinode/EIS wavelengths. All the APAP data are directly or indirectly included in a wide range of atomic databases and used by most of the astrophysics communities.

Transitions from high-n ($n = 4, 5, 6, 7$) states of iron and other elements are observed in the X-rays and soft X-rays, but little atomic data have been available. At Cambridge, we are currently calculating atomic data for a range of iron ions using a new development of the AUTOSTRUCTURE code, described in [21] to obtain collisional and radiative data for levels up to $n = 7$. The code uses the Breit-Pauli distorted wave approach and differs fundamentally from the well-known UCL-DW code.

CHIANTI

The CHIANTI (*www.chiantidatabase.org*) atomic database and associated programs [22] has become so successful (over 1000 citations) because it includes observed wavelengths, and all the necessary data to calculate line and continuum emissivities in a transparent and user-friendly way. All the atomic data are assessed (within a published manuscript) and extensive references to the original sources is given. This is a fundamental issue for the survival of atomic physics calculations (unfortunately, most atomic calculations are not properly referenced in the literature). The further inclusion of basic CHIANTI atomic data into further databases or modeling codes (e.g.: XSTAR, ATOMDB, XSPEC, ISIS, PINTofALE, CLOUDY, MOCASSIN) makes the problem worse.

The fundamental CHIANTI data include wavelengths, transition probabilities and spline fits [in the scaled domain of 23] to Maxwellian-averaged electron collision strengths. In version 6 [24], new ionization and recombination (radiative and dielectronic) rates have been included. We are currently in the process of designing a new format for the CHIANTI database and new software to overcome various current limitations. This will be implemented in version 8. The next version 7 [25] includes important updates for a range of ions, mostly for the EUV.

There are other ways in which atomic data are being made available. Basic atomic data and derived products were made available to the Virtual Observatory via the VOTADA project (G.Del Zanna) and Astrogrid (*http://www2.astrogrid.org/*) (UK funded). The Virtual Atomic and Molecular Data Centre (VAMDC, see *www.vamdc.eu*) has adopted a similar approach, aiming at building an interoperable e-infrastructure for the exchange of atomic and molecular data. VAMDC involves 15 administrative partners representing 24 teams from 6 European Union member-states, Serbia, the Russian Federation and Venezuela. Existing databases (e.g. CHIANTI) have been included into relational databases and linked within an infrastructure tuned to the requirements of a wide variety

of users in academic, governmental, and industrial communities.

BENCHMARK METHOD

Since 2003, I have embarked in a long-term project of benchmarking atomic data. All previous identifications and atomic calculations have been reviewed and assessed using the following method [see 17, for details]:

- find the best target and run atomic structure calculations using SUPERSTRUCTURE [26, 27]. Build a model ion that includes the most important configurations, applying semi-empirical adjustments (e.g. Term Energy Corrections to the LS energies) when needed.
- Use published excitation rates or calculate them with the R-matrix codes, using the best target.
- Calculate the level populations by including all the important cascading and excitation processes.
- Use a variety of sources of experimental data, calibrated independently from the atomic data.
- Try to identify all the brightest lines for each ion spanning the broadest spectral range.
- Compare both calculated and observed wavelengths and line intensities. Transition probabilities are also benchmarked with lifetimes measured with beam-foil spectroscopy.

The line intensities are compared in different regimes (low densities typical of the quiet solar corona and high-densities typical of laboratory spectra), using the 'emissivity ratio' method, whereby the observed intensity of a line is divided by its emissivity:

$$F_{ji} = \frac{I_{\rm ob}\, N_{\rm e}\, C}{N_j(N_{\rm e}, T_{\rm e})\, A_{ji}} \tag{1}$$

calculated at a fixed electron temperature $T_{\rm e}$ (or density $N_{\rm e}$) and plotted as a function of the density $N_{\rm e}$ (or temperature $T_{\rm e}$). $I_{\rm ob}$ is the observed intensity in the line. The scaling constant C is chosen so the curves are close to unity. The same constant is chosen for each dataset. If there is agreement between theory and observations, all the F_{ji} curves should either overlap or cross for nearly isodensity and isothermal plasmas. This allows, in one single plot, to assess at once for a group of lines how good observed vs. theoretical intensities are, hence assess the accuracy of the atomic calculations.

Various authors use some form of emission measure modelling to assess blending of spectral lines. For example, the integrated line intensity can be written as:

$$I(\lambda_{ji}) = \int_h N_{\rm e} N_{\rm H} A(X)\, G(N_{\rm e}, T, \lambda_{j,i}) dh \tag{2}$$

where $G(N_{\rm e}, T, \lambda_{j,i})$ is the *contribution function*, $N_{\rm H}$, $N_{\rm e}$ are the hydrogen and electron number densities, and the integral is on the line of sight dh. $A(X)$ is the elemental

abundance. If the plasma has a continuous distribution, a differential emission measure $DEM(T) = N_e N_H \frac{dh}{dT}$ can be defined, and spectral line intensities can then be estimated

$$I(\lambda_{ij}) = A(X) \int_T G(T)\, DEM(T)\, dT \tag{3}$$

However, large (and still unexplained) discrepancies are present in the emission measures of lines from different ions formed at similar temperatures. For a review of the various and often ignored complexities see [28].

With the new benchmark method, a large number of new lines and energy levels have been identified and given uncertainties. The best line ratios for density or temperature diagnostics are highlighted. The benchmark method also produced the discovery of several new diagnostic line ratios to measure electron densities and temperatures.

A large number of wavelengths have also been revised. In the literature, the most common reference values are e from the National Institute of Science and Technology (NIST) Atomic Spectra Database. This is largely a compilation which relies on original identifications and wavelength measurements performed in the 60's and 70's (or earlier), and they do not always provide the best values.

EIS was radiometrically calibrated on the ground [29] with an accuracy of about 20%, and can provide wavelengths with an accuracy of about 5 m Å, close to the best ever achieved, by [30] who provided a whole-Sun spectrum in the 160-770 Å range with excellent resolution (0.06 Å). EIS can also provide spatially-resolved monochromatic images which are extremely useful to identify the approximate formation temperature of each spectral lines which is a fundamental aid in the identification process [approximately half of the spectral lines still remain unidentified]. EIS is therefore well-suited for benchmarking atomic data. [31] provided an extensive list of lines observed with Hinode/EIS, but line identifications were not substantiated with a quantitative analysis.

The benchmark for Fe VII, Fe IX [32], Fe VIII [15], Fe XI [33], Fe XIII [34] has recently been done using Hinode/EIS spectra. The benchmark of Fe X [17] and Fe XII [35] was done with limited experimental data before Hinode was launched. A review of the main flare lines was given in [36], while a complete review of Fe XVII lines, with new identifications was given in [37]. An atlas of all the spectral lines emitted below 1 MK was provided in [32], while a full list of all the coronal lines has been given in [38], where all the coronal ions have been benchmarked.

Examples: Fe XI and Fe XVIII

After six years of benchmark work on the ions along the S-like sequence, the mysteries about some among the strongest lines in Fe XI have been unveiled. Three $J = 1$ levels in the $3s^2\ 3p^3\ 3d$ electron configuration give rise to strong lines in the EUV spectrum and their energies and identifications have been the source of much confusion in the literature. All previous atomic calculations produced discrepancies of factors 2-3 for these lines. A new R-matrix scattering calculation for electron collisional excitation of Fe XI by [18] has finally brought agreement, and allowed the firm identification of most of the $3s^2\ 3p^3\ 3d$ levels and of new temperature diagnostics [33].

Fe XVIII produces, in the X-ray and extreme ultraviolet, L-shell ($n = 2,3,4 \rightarrow 2$) spectral lines which are among the brightest ones. There has always been a discrepancy of factors 2-3 between observed and predicted intensities for the very bright $3s \rightarrow 2p$ transitions. The first large-scale R-matrix scattering calculations of [39] have finally resolved this puzzle. In this case, it turned out that the effect of the resonances was very important. A benchmark work [40] showed excellent agreement between observed and predicted intensities for the first time. Also, it provided new important diagnostics to measure electron temperatures and densities.

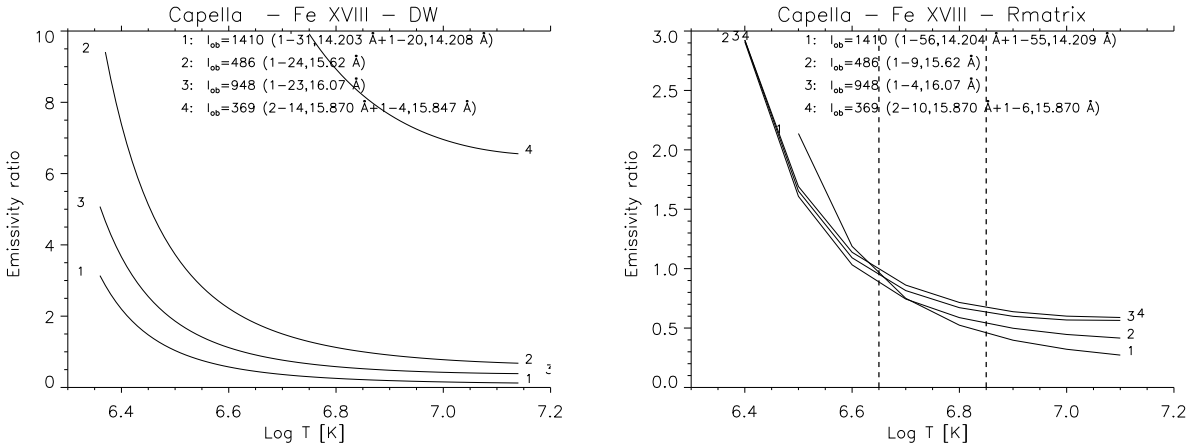

FIGURE 1. The emissivity ratio curves for the strongest Fe XVIII X-ray lines. Left, previous DW calculations; right: first R-matrix calculations.

Fig. 1 shows the emissivity ratio curves using the R-matrix results (right) and spectroscopic observations by Chandra of Capella [41]. The curves intersect at log T[K] =6.65, meaning that the line intensities can be explained, to with a few percent accuracy, by an isothermal plasma at a temperature well below that of peak abundance in ionization equilibrium (T[K] =6.85). On the other hand, previous distorted-wave (DW) atomic data [42] show a very large discrepancy.

ACKNOWLEDGMENTS

Support from STFC (UK) via the Advanced Fellowship programme is acknowledged. The work of the UK APAP Network was funded by the UK STFC under grant no. PP/E001254/1 with the University of Strathclyde. CHIANTI is a collaborative project involving the Universities of Cambridge (UK), George Mason and Michigan (USA). VAMDC is supported by the EU in the framework of the FP7 "Research Infrastructures-INFRA-2008-1.2.2 - Scientific Data Infrastructures" initiative.

REFERENCES

1. J. L. Culhane, L. K. Harra, A. M. James, K. Al-Janabi, L. J. Bradley, R. A. Chaudry, K. Rees, J. A. Tandy, P. Thomas, M. C. R. Whillock, B. Winter, G. A. Doschek, C. M. Korendyke, C. M. Brown, S. Myers, J. Mariska, J. Seely, J. Lang, B. J. Kent, B. M. Shaughnessy, P. R. Young, G. M. Simnett,

C. M. Castelli, S. Mahmoud, H. Mapson-Menard, B. J. Probyn, R. J. Thomas, J. Davila, K. Dere, D. Windt, J. Shea, R. Hagood, R. Moye, H. Hara, T. Watanabe, K. Matsuzaki, T. Kosugi, V. Hansteen, and Ø. Wikstol, *Sol. Phys.* pp. 60–+ (2007).
2. T. N. Woods, F. G. Eparvier, R. Hock, A. R. Jones, D. Woodraska, D. Judge, L. Didkovsky, J. Lean, J. Mariska, H. Warren, D. McMullin, P. Chamberlin, G. Berthiaume, S. Bailey, T. Fuller-Rowell, J. Sojka, W. K. Tobiska, and R. Viereck, *Sol. Phys.* pp. 3–+ (2010).
3. N. R. Badnell, *Journal of Physics B Atomic Molecular Physics* **30**, 1–11 (1997).
4. D. G. Hummer, K. A. Berrington, W. Eissner, A. K. Pradhan, H. E. Saraph, and J. A. Tully, *A&A* **279**, 298–309 (1993).
5. K. A. Berrington, W. B. Eissner, and P. H. Norrington, *Computer Physics Communications* **92**, 290–420 (1995).
6. N. R. Badnell, and D. C. Griffin, *Journal of Physics B Atomic Molecular Physics* **34**, 681–697 (2001).
7. N. R. Badnell, D. C. Griffin, and D. M. Mitnik, *Journal of Physics B Atomic Molecular Physics* **34**, 5071–5085 (2001).
8. M. C. Witthoeft, G. Del Zanna, and N. R. Badnell, *A&A* **466**, 763–770 (2007).
9. G. Y. Liang, A. D. Whiteford, and N. R. Badnell, *A&A* **500**, 1263–1269 (2009).
10. G. Y. Liang, and N. R. Badnell, *A&A* **518**, A64+ (2010).
11. G. Y. Liang, and N. R. Badnell, *A&A* **528**, A69+ (2011).
12. G. Y. Liang, A. D. Whiteford, and N. R. Badnell, *A&A* **499**, 943–954 (2009).
13. G. Y. Liang, N. R. Badnell, J. R. Crespo López-Urrutia, T. M. Baumann, G. Del Zanna, P. J. Storey, H. Tawara, and J. Ullrich, *ApJS* **190**, 322–333 (2010).
14. M. C. Witthoeft, and N. R. Badnell, *A&A* **481**, 543–551 (2008).
15. G. Del Zanna, *A&A* **508**, 513–524 (2009).
16. P. J. Storey, C. J. Zeippen, and M. Le Dourneuf, *A&A* **394**, 753–762 (2002).
17. G. Del Zanna, K. A. Berrington, and H. E. Mason, *A&A* **422**, 731–749 (2004).
18. G. Del Zanna, P. J. Storey, and H. E. Mason, *A&A* **514**, A40+ (2010).
19. P. J. Storey, G. Del Zanna, H. E. Mason, and C. Zeippen, *A&A* **433**, 717 (2005).
20. P. J. Storey, and C. J. Zeippen, *A&A* **511**, A78+ (2010).
21. N. R. Badnell, *Computer Physics Communications* **182**, 1528–1535 (2011).
22. K. P. Dere, E. Landi, H. E. Mason, B. C. Monsignori Fossi, and P. R. Young, *A&AS* **125**, 149–173 (1997).
23. A. Burgess, and J. A. Tully, *A&A* **254**, 436–+ (1992).
24. K. P. Dere, E. Landi, P. R. Young, G. Del Zanna, H. E. Mason, and M. Landini, *A&A* **498**, 915 (2009).
25. E. Landi, G. Del Zanna, P. R. Young, K. P. Dere, and H. E. Mason, *ApJ* p. submitted (2011).
26. W. Eissner, M. Jones, and H. Nussbaumer, *Computer Physics Communications* **8**, 270–306 (1974).
27. H. Nussbaumer, and P. J. Storey, *A&A* **64**, 139–144 (1978).
28. G. Del Zanna, M. Landini, and H. E. Mason, *A&A* **385**, 968–985 (2002).
29. J. Lang, B. J. Kent, W. Paustian, C. M. Brown, C. Keyser, M. R. Anderson, G. C. R. Case, R. A. Chaudry, A. M. James, C. M. Korendyke, C. D. Pike, B. J. Probyn, D. J. Rippington, J. F. Seely, J. A. Tandy, and M. C. R. Whillock, *Appl. Opt.* **45**, 8689–8705 (2006).
30. W. E. Behring, L. Cohen, G. A. Doschek, and U. Feldman, *ApJ* **203**, 521–527 (1976).
31. C. M. Brown, U. Feldman, J. F. Seely, C. M. Korendyke, and H. Hara, *ApJS* **176**, 511–535 (2008).
32. G. Del Zanna, *A&A* **508**, 501–511 (2009).
33. G. Del Zanna, *A&A* **514**, A41+ (2010).
34. G. Del Zanna, *A&A* accepted (2011).
35. G. Del Zanna, and H. E. Mason, *A&A* **433**, 731 (2005).
36. G. Del Zanna, *A&A* **481**, L69–L72 (2008).
37. G. Del Zanna, and Y. Ishikawa, *A&A* **508**, 1517–1526 (2009).
38. G. Del Zanna, *A&A* submitted (2011).
39. M. C. Witthoeft, N. R. Badnell, G. del Zanna, K. A. Berrington, and J. C. Pelan, *A&A* **446**, 361–366 (2006).
40. G. Del Zanna, *A&A* **459**, 307 (2006).
41. K. J. H. Phillips, M. Mathioudakis, D. P. Huenemoerder, D. R. Williams, M. E. Phillips, and F. P. Keenan, *MNRAS* **325**, 1500–1510 (2001).
42. D. H. Sampson, H. L. Zhang, and C. J. Fontes, *Atomic Data and Nuclear Data Tables* **48**, 25–+ (1991).